The Effect of Electric Fields on Silicon-Based Monolayers

Tiexin Li[1], Chandramalika Peiris[1], Essam M. Dief[1], Melanie MacGregor[2], Simone Ciampi[1] & Nadim Darwish[1]*

[1]*School of Molecular and Life Sciences, Curtin University, Bentley, WA 6102, Australia*

[2]*Flinders Institute for Nanoscale Science & Technology, Flinders University, Bedford Park, SA 5042, Australia*

**Corresponding author: nadim.darwish@curtin.edu.au*

ABSTRACT

Electric fields can induce bond breaking, bond forming, catalyse chemical reactions on surfaces, and change the structure of self-assembled monolayers (SAMs) on electrode surfaces. Here, we study the effect of electric fields supplied either by an electrochemical potential or by conducting atomic force microscopy (C–AFM) on Si-based monolayers. We report that typical monolayers on silicon undergo partial desorption, followed by oxidation of the underneath silicon at + 1.5 V vs Ag/AgCl. The monolayer loses 28% of surface coverage and 55% of its electron transfer rate constant (k_{et}) when + 1.5 V electrochemical potential is applied on the Si surface for 10 minutes. Similarly, a bias-voltage of + 5 V applied by C–AFM, induces complete desorption of the monolayer at specific sites accompanied by an average oxide growth of 2.6 nm when the duration of the bias applied is 8 minutes. Current–voltage plots progressively changes from rectifying typical of metal–semiconductor junctions to insulating as the oxide grows. These results define the stability of Si-based organic monolayers toward electric fields and have implication in the design of silicon-based monolayers, molecular electronics devices, and on the interpretation of charge transfer kinetics across them.

1. INTRODUCTION

Electric fields are known to break and form chemical bonding,[1] catalyse chemical reactions, induce the formation of compact double layer of ionic liquids on surfaces,[2] and change the structure of self-assembled monolayers.[3] For instance, thiol-based monolayers on gold were shown to undergo structural changes involving a change from a tilted alkyl-chain orientation to a more perpendicular position with applied electric fields.[4] The reason for this monolayer twisting is electric-field induced torque on the S–Au bonding which forces the molecules to align with the surface normal.[4]

Monolayers on gold have been so popular for a range of applications, such as biosensors,[5-10] surface patterning,[11-14] various chemical and biological surface functionalizations[15-19] and, fundamental electron transfer studies.[20-21] However more recently, monolayers on silicon is increasingly gaining attention.[22-34] Typical monolayers on silicon forms covalent bonding between silicon and molecules via Si–O,[35-37] Si–S[38-41] and, Si–C[42-45] bonding. These robust monolayers offers new opportunities for microelectronics in which traditional silicon electronics can be combined with molecular electronics.[46-50] Monolayers on silicon is believed to form protective film that prevent the underneath silicon from oxidation.[51-52] In this study, we ask the question as to what extent can these monolayers protect the film from electric fields during typical electrochemical and electrical measurements.

We systematically study the effect of electric fields supplied by electrochemical potentials at the Si–electrolyte interface or by voltage-biases supplied by C–AFM on a SAM formed from nonadiyne which is known to form a high quality monolayer on Si. In the electrochemical system, potentials of + 0.6 , + 1 , and + 1.5 V are applied, whereas in C–AFM system, the Si surface is biased against the tip at + 1 , + 2 , + 3 and, + 5 V. Electrochemical techniques, such as cyclic voltammetry (CV) and electrochemical impedance spectroscopy (EIS), are used to

determine the molecular surface coverage and electron transfer kinetics. Contact angle goniometry was used to follow the surface functional groups and voltage–current electrical measurements were used to assess the electrical properties of the oxide formed.

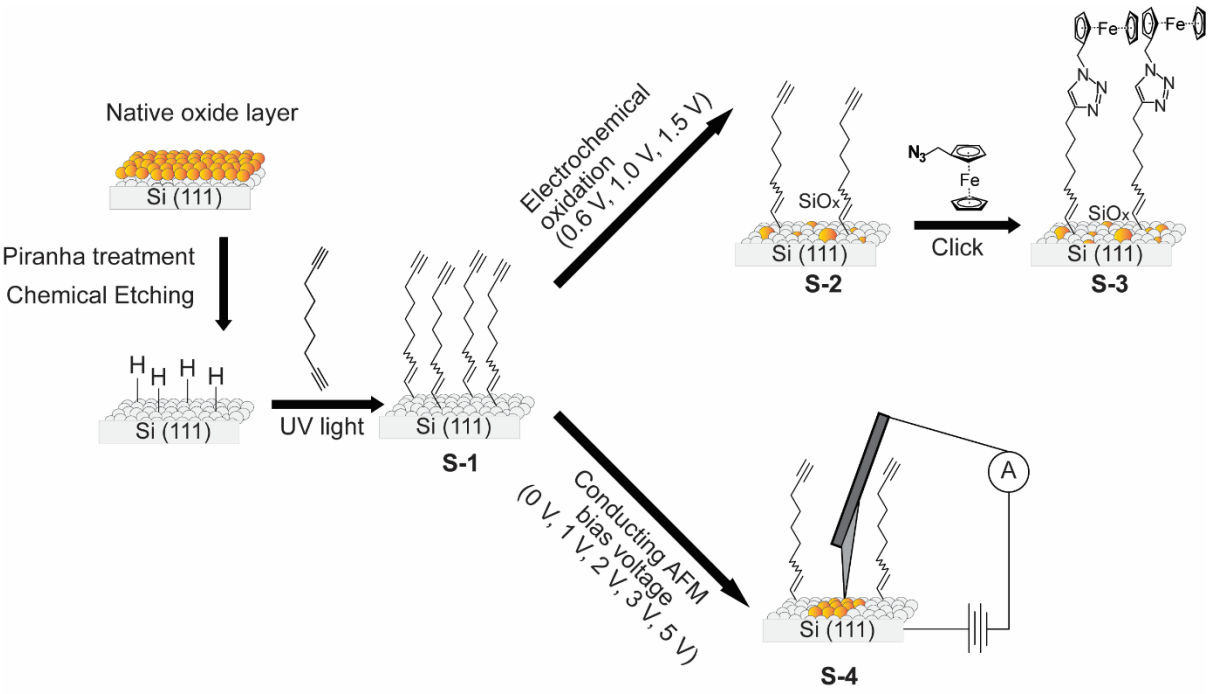

Figure 1. Schematic of the SAMs studied. Oxide-free silicon (Si–H) electrodes are reacted with 1,8-nonadiyne via a hydrosilylation reaction to form SAM **S-1**. Electrochemical potentials of + 0.6, + 1.0, and + 1.5 V are then applied to SAM **S-1** form SAM **S-2**. A ferrocene moiety is attached to the distal end of **S-2** monolayer by a copper-catalyzed azide-alkyne "click" reaction to yield the redox-active SAM **S-3**. On the other hand, C-AFM induced oxidation of SAM **S-1** was obtained by applying + 1, + 2, + 3 and, + 5 V bias-voltage to yield SAM **S-4**. The schematic assumes that the oxide grows progressively from the molecular scale to the nanoscale and then to the microscale.

2. MATERIALS AND METHODS

2.1 Materials

Unless specified otherwise, all chemicals were of analytical grade and used as received. Chemicals used in surface modification and electrochemical experiments were of high purity

(>99%). Milli–Q water (>18 MΩ cm) was used for surface cleaning, glassware cleaning and for the preparation of the electrolyte solutions. Dichloromethane (DCM) and 2–propanol were distilled before use. Hydrogen peroxide (30 wt% in water), sulfuric acid (Puranal TM, 95–97%) and ammonium fluoride (Puranal TM, 40 wt% in water) were of semiconductor grade and were used for silicon-wafer cleaning and etching. 1,8–Nonadiyne (98%) was obtained from Sigma-Aldrich and used as received. Azidomethylferrocene was synthesised from ferrocene methanol using a literature procedure.[53] Aqueous perchloric acid (1.0 M) was used as the electrolyte in all electrochemical measurements. Silicon wafers were purchased from Siltronix, S.A.S. (Archamps, France), p-type boron doped, and had a thickness of 500 ± 25 μm and a resistivity of 0.007–0.013 Ω cm.

2.2 Surface Modification

2.2.1 Silicon passivation. The hydrosilylation reaction of 1,8–nonadiyne with Si–H followed a previously reported procedure.[53-54] In brief, silicon wafers were cut into pieces (approximately 1 × 1 cm), cleaned in hot Piranha solution (130 °C, 3:1(v/v) mixture of concentrated sulfuric acid to 30% hydrogen peroxide) for 20 minutes, then rinsed with water and etched in deoxygenated (40 wt%) aqueous ammonium fluoride solution under a stream of argon for 13 minutes. The etched samples were rinsed with Milli–Q water and DCM before being placed in a deoxygenated sample of 1,8–nonadiyne. The surfaces were then rapidly transferred to a reaction chamber kept under nitrogen flow, and illuminated with UV light (Vilber, VL–215.M, λ = 312 nm) for 2 hours.

2.2.2 Electrochemical oxidation. Amperometric I-T measurements were run at different voltage (+ 0.6, + 1, and + 1.5 V) for 1 minute, 5 minutes, and 10 minutes. The 1,8–nonadiyne SAMs served as working electrode, a platinum wire as the auxiliary electrode, and an Ag/AgCl

aqueous electrode (1.0 M KCl, CH Instruments, USA) as the reference electrode. Aqueous 1.0 M perchloric acid was used as the electrolyte.

2.2.3 Copper-catalysed azide–alkyne "click" reaction. The oxidized 1,8–nonadiyne SAMs (**S-2**, Figure 1) were reacted with azidomethylferrocene through a copper-catalysed "click" reaction to yield SAM **S-3**. In brief, **S-2** samples were incubated in a solution of 0.4 μM copper (II) sulphate pentahydrate, sodium ascorbate (5 mg/mL) and 0.5 mM azidomethylferrocene, under dark conditions. The reaction time was 120 minutes. The silicon substrates were then removed from the solution and washed sequentially with 2-propanol, Milli-Q water, 0.5 M hydrochloric acid, Milli-Q water, 2-propanol and DCM. Finally, the silicon substrates (**S-3**) were blown dry with a stream of argon before analysis.

2.3. Surface characterization

2.3.1 Electrochemical measurements. Electrochemical measurements were carried out in a single-compartment, three-electrode PTFE cell using a CHI650 electrochemical workstation (CH Instruments, USA). The modified silicon surface served as the working electrode, a platinum wire as the auxiliary electrode, and an Ag/AgCl aqueous electrode (1.0 M KCl, CH Instruments, USA) as the reference electrode. Aqueous 1.0 M perchloric acid was used as the electrolyte. The electrical contact between silicon and copper was reached by rapidly rubbing gallium indium eutectic on the back side of the silicon substrate. EIS measurements were carried out with a DC offset equal to the half-wave potential ($E_{1/2}$) measured in the CV experiments. The AC amplitude was 15 mV and the frequency was scanned between 0.1 and 100,000 Hz. The surface coverages (Γ) of ferrocene molecules was calculated from the integration of the CV oxidation waves according to $\Gamma=Q/nFA$ (where Q is charge, n is number of electron transfer, F is Faraday constant and A is area of electrode).

2.3.2 Atomic Force Microscopy (AFM). All the topography imaging were conducted on Bruker Dimension FastScan atomic force microscopy in air and at room temperature. All the AFM data was processed with NanoScope Analysis. The antimony (n) doped silicon tips (TESPA-V2, Bruker AFM Probes), with spring constant of 42 N/m and resonance frequency of 320 kHz, were used to probe the sample topography. The measurements were performed in tapping mode while the size of image was set to 5×5 μm^2, the resolution to 256 points/line and the scan rate to 1.0 Hz.

2.3.3 Conductive Atomic Force Microscope (C–AFM). Tip induced oxidation was performed on Bruker Dimension PF–TUNA atomic force microscopy in the ambient conditions (21 ℃ and 30% relative humidity). All images and current–voltage (I–V) curves were obtained with solid Pt tips (RMN–25PT300B, Rocky Mountain Nanotechnology), with nominal spring constant of 18 N/m, nominal resonant frequency of 20 kHz, and tip radius < 20 nm in air at room temperature. The silicon wafers were oxidised by applied biases ranging from 1 to 5 V. I–V curves were obtained by ramping 20 times in each position at a peak force of 2.25 μN and 1 Hz ramp rate.

2.3.4 Contact angle analysis. The wettability of the Si surfaces was measured by an automated static water contact angle with a Krüss DSA 100 goniometer. The reported values are the average of at least three droplets, and the error bars represent the standard deviation of three measurements on three different surfaces.

3. RESULTS AND DISCUSSION

3.1. Electrochemical Studies

We first tested the effect of electrochemical potential on the topography of the monolayer. For this purpose a monolayer of 1,8–nonadiyne on Si is constructed via a hydrosilylation reaction.

An electrochemical potential of + 0.6, + 1 and, + 1.5 V is then applied to the surface. The surfaces were then imaged by tapping-mode AFM.

A freshly prepared **S–1** surface showed clearly visible Si (111) flat terraces with smooth edges, of peak-to-peak surface roughness within individual terrace of ~ 0.245 nm, and negligible oxide (Figure 2a). When a potential of + 0.6 V was applied to the **S-1** SAM for 1 minute, clear oxide spots appears and the terraces become less visible (Figure 2b). After applying + 1.5 V for 10 minutes, the surfaces show clear oxide spots and Si (111) terraces become increasingly invisible (Figure 2c).

Figure 2d–f show the water wettability of the SAM S-1 before and after applying the electrochemical potential. Initially SAM S-1 has a contact angle of 77 °, which is reduced to 64 ° and 48 ° when + 0.6, and + 1.5 V, are applied for 1 and 10 minutes, respectively. This is likely due to the oxide growth resulting in higher surface-polarity. The contact angle of SAM **S-1** is 77 ° meaning the surface is relatively more hydrophobic. As a comparison, the contact angle of 1,8-nonadiyne on a gold surface is 71 ° (Figure S5), which suggests that the monolayer is slightly more dense on silicon than it is on gold. Figure 2g shows the XPS Si 2p narrow scan for a freshly prepared surface, a surface oxidized at + 0.6 V, and a surface oxidized at + 1.5 V. Freshly prepared surface **S-1** show only limited amount of SiO_x at 102 eV (7%), (Figure 2g) and increases to 13% and 29% when the voltage increased from + 0.6 V (applied for 1 minute) to +1.5 V (applied for 10 minutes), respectively (Figure 2h-i). The Si 2p high resolution envelope was fitted by four peaks, with the main emission composed of one spin-orbit split with two peaks at 98.85 eV and 99.45 eV, corresponding to the Si $2p_{3/2}$ and Si $2p_{1/2}$ for low and high energy spins, respectively. The two small peaks at 99.20 eV and 99.85 eV are Si–C at and Si–O, respectively and are attributed to carbon and oxygen from the measurement's environment.[55] The survey XPS spectra for **S-1** SAM are shown in Figure S9 (Supporting Information).

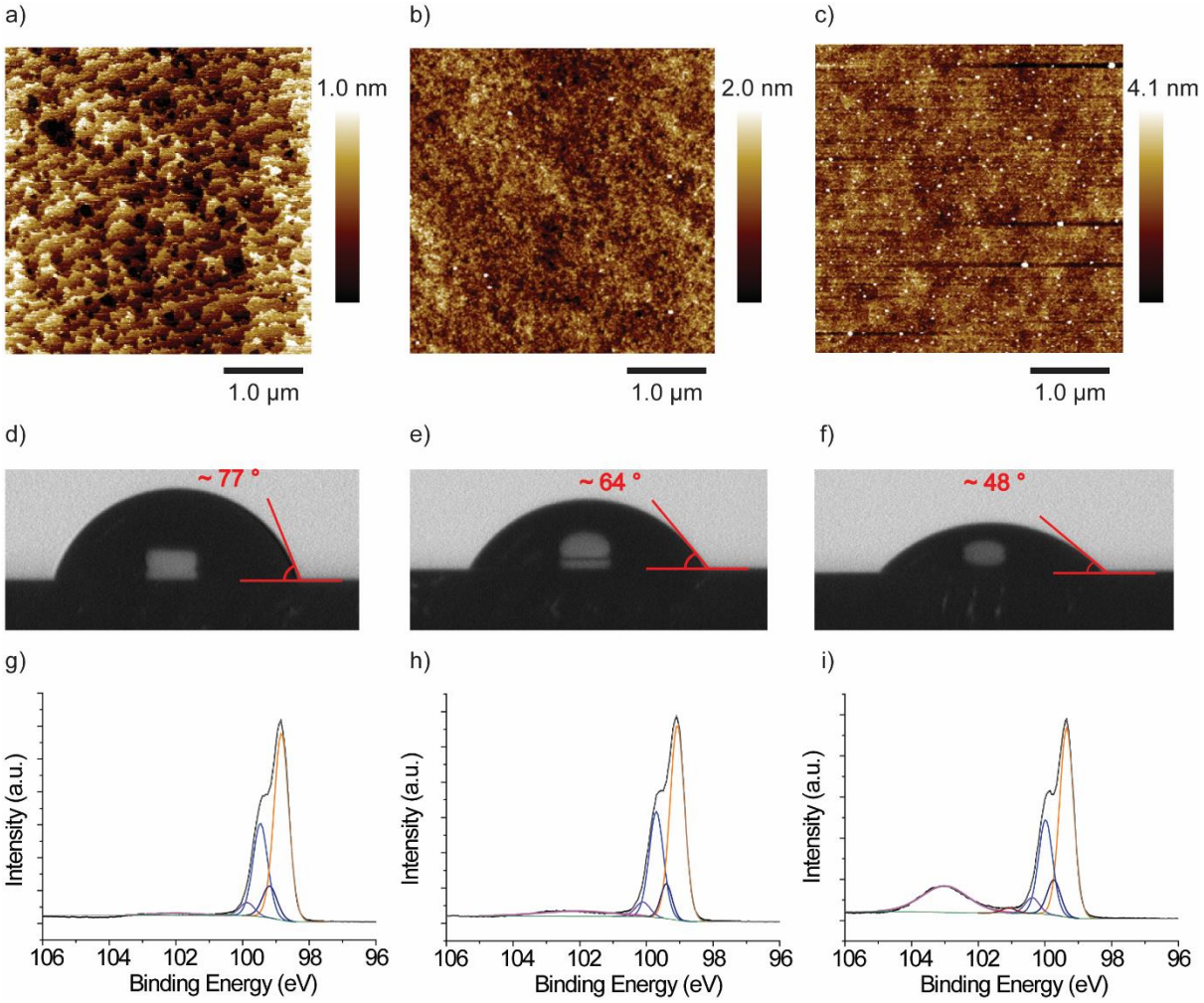

Figure 2. a) AFM topography images for **S-1** SAM in a fresh state. b) AFM topography images of SAM **S-2** obtained after an electrochemical potential of 0.6 V was applied to SAM **S-1** for 1 minute. c) AFM topography images of SAM **S-2** after applying an electrochemical potential of +1.5 V to SAM **S-1** for 10 minutes. d) The static image of a water droplet on a freshly prepared SAM **S-1**. e) The static image of a water droplet on SAM **S-2**, which is obtained after an electrochemical potential of +0.6 V was applied to SAM **S-1** for 1 minute. f) The static image of a water droplet on SAM **S-2**, which is obtained after an electrochemical potential of +1.5 V was applied to SAM **S-1** for 10 minutes. XPS high resolution Si 2p spectra for **S-1** SAM (g) freshly prepared, (h) oxidized at +0.6 V, and (i) oxidized at + 1.5 V.

Next, we measured the surface coverage after applying + 0.6, + 1.0 and + 1.5 V. For this purpose, the potential was first applied to SAM **S–1** for a specific amount of time. The SAM was then reacted with azidomethylferrocene via an azide-alkyne "click" reaction yielding SAM **S-3**. The purpose of the ferrocene moieties is to enable determining the surface coverage, electrochemically.

Figure 3a–c show the CVs for **S–3** SAM after applying to the **S–1** SAM, a potential of + 0.6 , + 1.0 , and + 1.5 V for 1 minute, 5 minutes, and 10 minutes. The CVs show the characteristic redox peaks of the ferrocene moiety at 0.46 V vs Ag/AgCl. A key observation is the separation between the oxidation and reduction waves increases with the increase in the potential magnitude and duration. For example, the separation increases from 32 to 96 mV when the potential is increased from + 0.6 V for 1 minute to + 1.5 V for 10 minutes. In addition, the waves separation increases with the duration of the potential applied. For example, at + 1.5 V, the peak separation increases from 70 to 96 mV when the potential duration increases from 1 to 10 minutes. The increase in waves separation is an indication of slower electron-transfer kinetics.[56]

Another key observation from the CVs is the decrease in surface coverage with the magnitude and duration of the applied potential. The surface coverage of SAM **S-3** decrease from (1.05 ± 0.26) × 10^{14} ferrocene cm^{-2} to (7.36 ± 2.06) × 10^{13} ferrocene cm^{-2} when the applied potential increases from + 0.6 to + 1.5 V for the same duration of 1 minute (Figure 3d). The surface coverage also decreases with the duration of the applied potential with the coverage decreasing by ~ 28% from (7.36 ± 2.06) × 10^{13} ferrocene cm^{-2} to (5.27 ± 1.11) × 10^{13} ferrocene cm^{-2} when the duration of the + 1.5 V potential was increased from 1 to 10 minutes. The surface coverage of SAM **S-3** decreases from (1.39 ± 0.38) × 10^{14} ferrocene cm^{-2} to (1.03 ± 0.26) × 10^{14} ferrocene cm^{-2} when the applied potential increases from – 0.6 to – 1.5 V for 1 minute. When the potential of – 1.5 V applied increase from 1 to 10 minutes, the surface decreases from (1.03 ± 0.26) × 10^{14} ferrocene cm^{-2} to (8.24 ± 1.73) × 10^{13} ferrocene cm^{-2}. Similar effects were observed for a molecule that comprises a ferrocene moiety as opposed to the above post-click reaction method. Experiments with 11-(ferrocenyl)undecanethiol showed as similar trend of a decrease in surfaces coverage as a function of the increasing applied voltage (Figure S6a, Supporting Information).

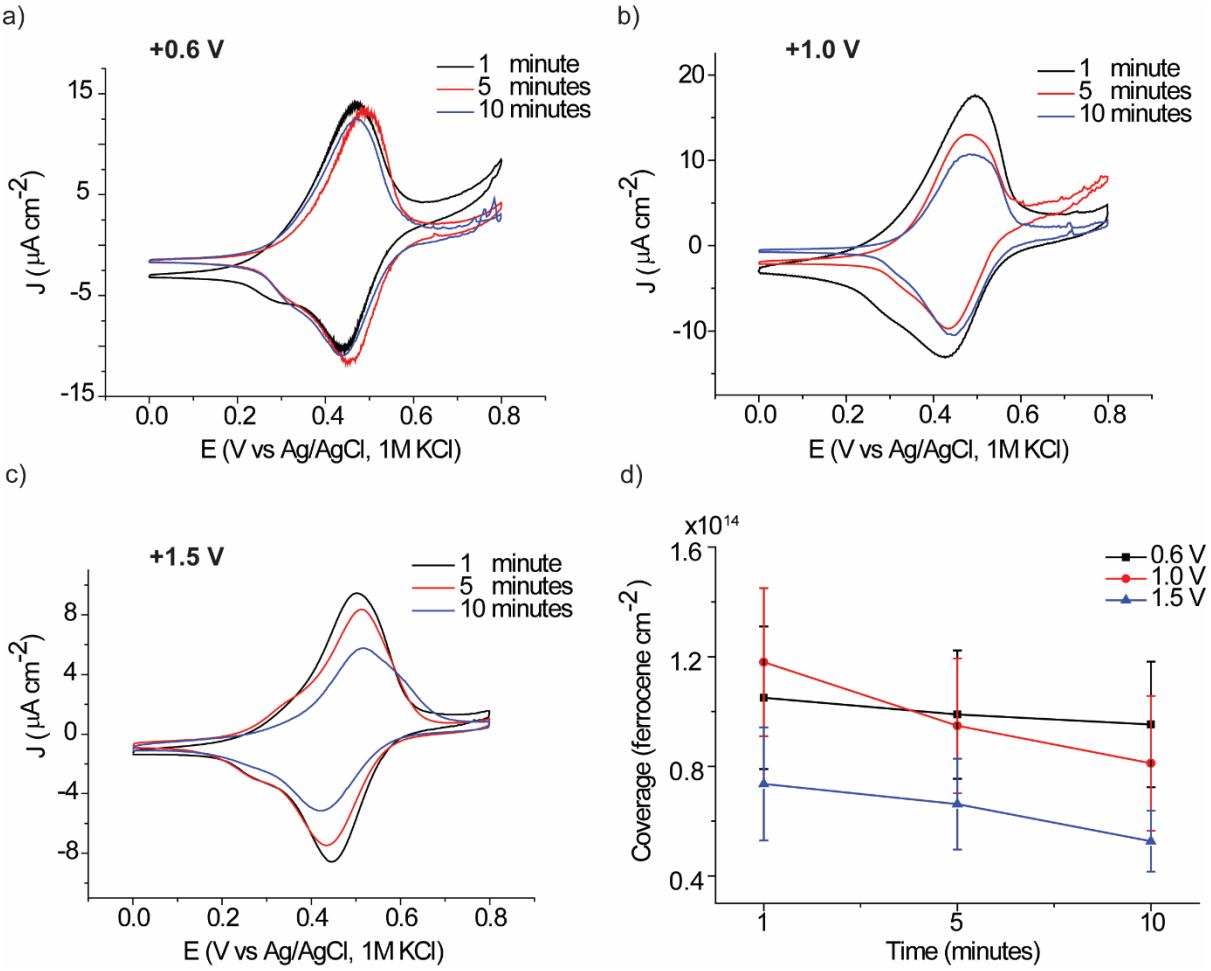

Figure 3. Cyclic voltammetry for SAM **S-3** which is obtained after applying to SAM **S-1** an electrochemical potential of a) + 0.6 V, b) + 1.0 V and, c) + 1.5 V for 1, 5 and 10 minutes, respectively, followed by an azide–alkyne click reaction with azidomethylferrocene d) The corresponding surface coverages calculated from the oxidation waves of the CVs in (a), (b), and (c). The error bars in (d) is the standard deviation of surface coverages from the mean value of three different surfaces.

To determine the charge transfer kinetics, electrochemical impedance spectroscopy (EIS) was performed on SAM **S–3** (Figure S1). Similar to the trend observed for the surface coverages, the electron transfer kinetics was shown to decrease with increasing potential magnitude and duration. For example the rate constants (k_{et}) decreases from (125.64 ± 4.24) to (5.72 ± 1.16) s^{-1} when the potential applied to SAM **S–1** increases from + 0.6 to + 1.5 V for 1 minute. In addition, the duration of the potential applied affects k_{et}. For instance, it decreases from (5.72

± 1.16) to (2.58 ± 0.45) s^{-1} when the duration of the potential pulse at + 1.5 V increases from 1 to 10 minutes. The k_{et} decrease from (132.99 ± 7.26) to (111.43 ± 3.82) s^{-1} when the applied potential increases from + 0.6 to + 1.5 V for the same duration of 1 minute. The k_{et} also decreases from (111.43 ± 3.82) to (37.48 ± 0.50) s^{-1} when the duration of the + 1.5 V potential was increased from 1 to 10 minutes. The oxidation could happen at both positive and negative voltages, and this is likely due to the ability of electric field to desorb the H for Si-H leading to Si radicals that can then react with oxygen and water forming the oxide. A similar trend of decrease in k_{et} have been also obtained for monolayers formed from 11-(ferrocenyl)undecanethiol (Figure S6b, Supporting Information). Full trends are presented in Figure 4a–f. Bode plots from EIS are shown in Figure S2 (Supporting Information).

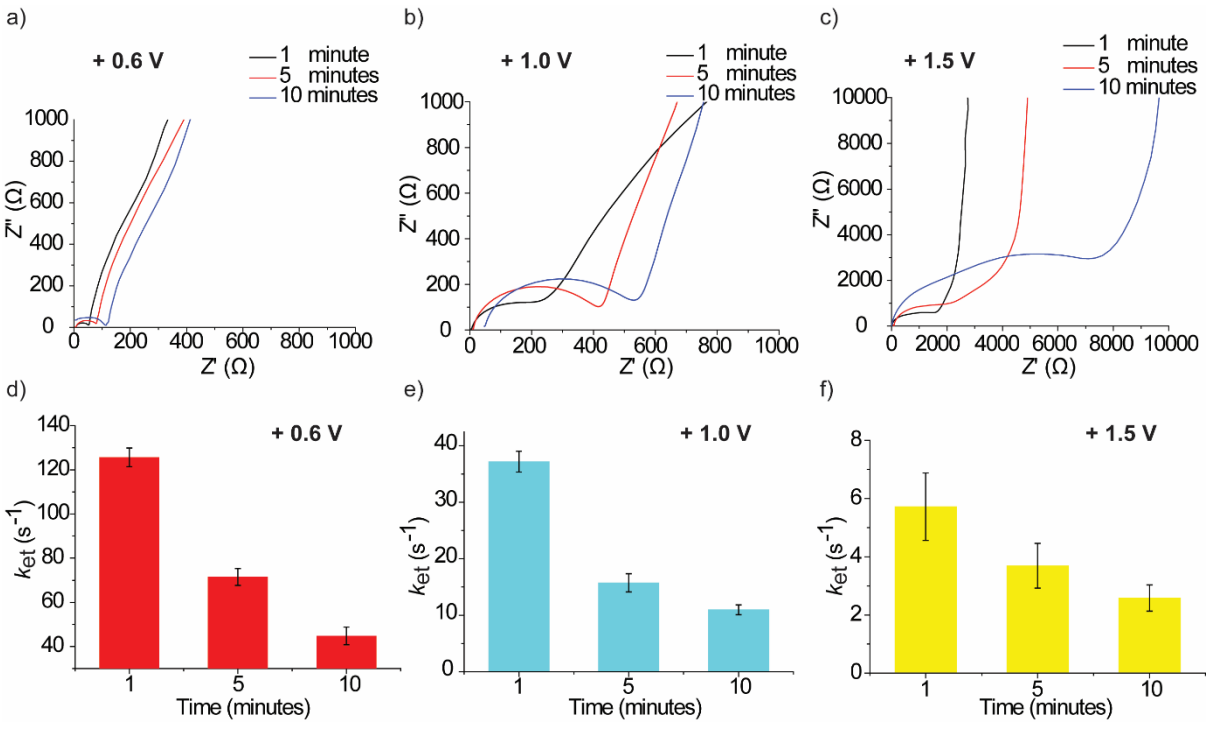

Figure 4. Nyquist plots from EIS measurements of SAM **S-3** which is obtained after applying to SAM **S-1** an electrochemical potential of a) + 0.6 V, b) + 1 V and, c) + 1.5 V for 1, 5 and 10 minutes, respectively, followed by an azide–alkyne click reaction with azidomethylferrocene. The corresponding evolution in k_{et} after d) + 0.6 V, e) + 1 V and, f) + 1.5 V was applied for 1, 5 and 10 minutes. The EIS fitting parameters are presented in Tables S1–S3 of the Supporting

Information. The error bars in (d), (e), and (f) are the standard deviation of k_{et} from the mean value of three different surfaces.

3.2. Conducting AFM studies

After performing the wet electrochemical experiments, we proceeded using C-AFM to test how a bias-voltage applied between a Pt AFM tip and the monolayer-modified Si surface (SAM **S–1**, Figure 5f-j) affects current–voltage measurements. These experiments differ from the electrochemical experiments (section 3.1) in that they are performed in dry conditions without an electrochemical control in aqueous environment. The bias-voltage between the tip and the surface was applied to surface **S–1** at specific location for 8 minutes. Topography images are then recorded at low bias-voltages to check what the effect of the previous bias-voltage applied was (Figure 5a-e). A key observation is the growth of oxide squares on SAM **S-1** and the oxide thickness significantly increase with the magnitude of the bias-voltages applied from (0.8 ± 0.06) nm to (2.6 ± 0.23) nm when the bias-voltage increases from + 1 V to + 5 V (Figure S3). In addition, I–V measurements were performed on and outside the oxide areas. When the bias voltage applied exceeded + 1 V, the resulting oxide growth affected the magnitude of the current compared to that recorded on unbiased surfaces (Figure 5k-o). In particular, the I–V curves change from a typical rectifying metal–semiconductor junction to nearly an insulator. Hence, care should be taken to analyse I–V curves of molecules on Si as biase-voltages as low as +1 V can create oxide, which will then dominate the measurements.

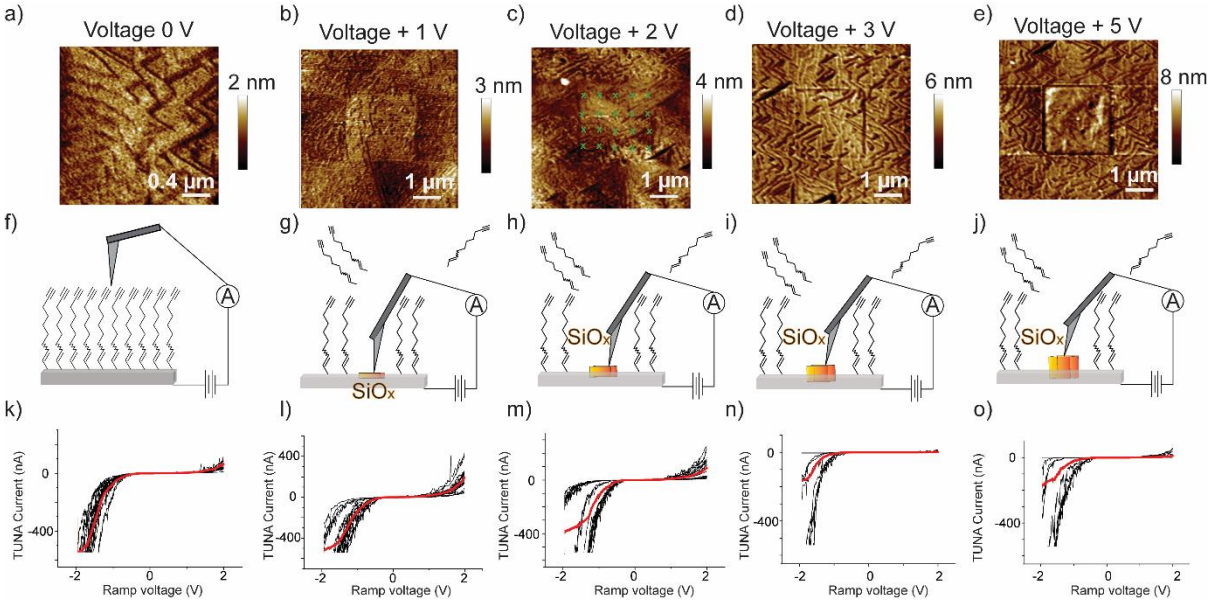

Figure 5. AFM topography of the oxide squares obtained on SAM **S-1** by AFM–tip induced oxidation at no bias-voltage (0 V) (a), + 1 V (b), + 2 V (c), + 3 V (d) and + 5 V (e). (f–j) Cartoons describing the respective experiments and each surfaces. I–V curves of the **S-1** surface biased at 0 V (k), + 1 V (l), + 2 V (m), + 3 V (n), + 5 V (o). The red line in Figure (k-o) is the average TUNA current for 20 curves. Positive bias means the Si is positively biased relative to the tip.

4. CONCLUSIONS

In summary, we demonstrate that electric fields have profound effect on silicon-based monolayers. Whether the electric fields are those encountered in typical 3–electrode electrochemical setups or those electrically induced using nanoscale electrical measurements, the electric fields partially desorb the organic monolayer from the Si surface and is accompanied by a growth of an oxide layer. The oxide growth leads to wave separation in cyclic voltammetry, decrease in the molecular surface coverage and decrease in the rate of electron transfer when a redox active group is attached to the terminal end of the monolayer. These results explain the scattered cyclic voltammetry and electron-transfer rate constant typically reported for surface-bound redox monolayers on Si. Equally important, is our demonstration that at the nanoscale, an oxide growth is observed by C-AFM when the Si

surface is biased by a voltage as low as + 1 V, above which the I–V curves show less currents reflecting the insulating properties of the oxide areas created underneath. These observations should be taken into account when designing molecular electronics devices on Si, which often requires scanning the bias voltage with magnitudes comparable to that applied in this study. The results also point out to the need to develop better monolayers on Si that can withstand high electric fields. The well-defined silicon oxide structures created over silicon by AFM tips could also find implications in understanding the properties of this type of silica for the design of memristors arrays.

SUPPORTING INFORMATION

Detailed contact angle, XPS and electrochemical analysis are supplied as Supporting Information.

DECLARATION OF COMPETING INTEREST

The authors declare no competing financial interest.

ACKOWLEDGEMENTS

The authors acknowledge support from the Australian Research Council (DP190100735).

5. REFERENCES

1. Pla-Vilanova, P.; Aragonès, A. C.; Ciampi, S.; Sanz, F.; Darwish, N.; Diez-Perez, I., The spontaneous formation of single-molecule junctions via terminal alkynes. *Nanotechnology* **2015,** *26* (38), 381001.

2. Zhang, Y.; Ye, T.; Chen, M.; Goodwin, Z. A.; Feng, G.; Huang, J.; Kornyshev, A. A., Enforced Freedom: Electric-Field-Induced Declustering of Ionic-Liquid Ions in the Electrical Double Layer. *Energy & Environmental Materials* **2020,** *3* (3), 414-420.

3. Heo, J.; Ahn, H.; Won, J.; Son, J. G.; Shon, H. K.; Lee, T. G.; Han, S. W.; Baik, M.-H., Electro-inductive effect: Electrodes as functional groups with tunable electronic properties. *Science* **2020,** *370* (6513), 214-219.

4. Darwish, N.; Eggers, P. K.; Ciampi, S.; Zhang, Y.; Tong, Y.; Ye, S.; Paddon-Row, M. N.; Gooding, J. J., Reversible potential-induced structural changes of alkanethiol monolayers on gold surfaces. *Electrochem. Commun.* **2011,** *13* (5), 387-390.

5. Li, Z.; Munro, K.; Ebralize, I. I.; Narouz, M. R.; Padmos, J. D.; Hao, H.; Crudden, C. M.; Horton, J. H., N-heterocyclic carbene self-assembled monolayers on gold as surface plasmon resonance biosensors. *Langmuir* **2017,** *33* (49), 13936-13944.

6. Losic, D.; Short, K.; Mitchell, J. G.; Lal, R.; Voelcker, N. H., AFM nanoindentations of diatom biosilica surfaces. *Langmuir* **2007,** *23* (9), 5014-5021.

7. Worsfold, O.; Voelcker, N. H.; Nishiya, T., Biosensing using lipid bilayers suspended on porous silicon. *Langmuir* **2006,** *22* (16), 7078-7083.

8. Jane, A.; Dronov, R.; Hodges, A.; Voelcker, N. H., Porous silicon biosensors on the advance. *Trends Biotechnol.* **2009,** *27* (4), 230-239.

9. Perera, H. G.; Lu, T.; Fu, L.; Zhang, J.; Chen, Z., Probing the Interfacial Interactions of Monoclonal and Bispecific Antibodies at the Silicone Oil–Aqueous Solution Interface by Using Sum Frequency Generation Vibrational Spectroscopy. *Langmuir* **2019,** *35* (44), 14339-14347.

10. Wu, Y.; Tilley, R. D.; Gooding, J. J., Challenges and solutions in developing ultrasensitive biosensors. *J. Am. Chem. Soc.* **2018,** *141* (3), 1162-1170.

11. Geissler, M.; McLellan, J. M.; Chen, J.; Xia, Y., Side-by-side patterning of multiple alkanethiolate monolayers on gold by edge-spreading lithography. *Angew. Chem.* **2005,** *117* (23), 3662-3666.

12. Vasani, R. B.; McInnes, S. J.; Cole, M. A.; Jani, A. M. M.; Ellis, A. V.; Voelcker, N. H., Stimulus-responsiveness and drug release from porous silicon films ATRP-grafted with poly (N-isopropylacrylamide). *Langmuir* **2011,** *27* (12), 7843-7853.

13. Hoffman, L. W.; Andersson, G. G.; Sharma, A.; Clarke, S. R.; Voelcker, N. H., New insights into the structure of PAMAM dendrimer/gold nanoparticle nanocomposites. *Langmuir* **2011,** *27* (11), 6759-6767.

14. Zhang, X.; Chen, X.; Yang, J.; Jia, H. R.; Li, Y. H.; Chen, Z.; Wu, F. G., Quaternized Silicon Nanoparticles with Polarity-Sensitive Fluorescence for Selectively Imaging and Killing Gram-Positive Bacteria. *Adv. Funct. Mater.* **2016,** *26* (33), 5958-5970.

15. Walkey, M. C.; Peiris, C. R.; Ciampi, S.; C. Aragonès, A.; Domínguez-Espíndola, R. B.; Jago, D.; Pulbrook, T.; Skelton, B. W.; Sobolev, A. N.; Díez Pérez, I., Chemically and mechanically controlled single-molecule switches using spiropyrans. *ACS Appl. Mater. Interfaces* **2019,** *11* (40), 36886-36894.

16. Darwish, N.; Díez-Pérez, I.; Da Silva, P.; Tao, N.; Gooding, J. J.; Paddon-Row, M. N., Observation of electrochemically controlled quantum interference in a single anthraquinone-based norbornylogous bridge molecule. *Angew. Chem. Int. Ed.* **2012,** *51* (13), 3203-3206.

17. Sweetman, M. J.; Shearer, C. J.; Shapter, J. G.; Voelcker, N. H., Dual silane surface functionalization for the selective attachment of human neuronal cells to porous silicon. *Langmuir* **2011,** *27* (15), 9497-9503.

18. Li, Y.; Pan, D.; Nashine, V.; Deshmukh, S.; Vig, B.; Chen, Z., Understanding protein-interface interactions of a fusion protein at silicone oil-water interface probed by sum frequency generation vibrational spectroscopy. *J. Pharm. Sci.* **2018,** *107* (2), 682-689.

19. Wu, F. G.; Zhang, X.; Kai, S.; Zhang, M.; Wang, H. Y.; Myers, J. N.; Weng, Y.; Liu, P.; Gu, N.; Chen, Z., One-step synthesis of superbright water-soluble silicon nanoparticles with

photoluminescence quantum yield exceeding 80%. *Adv. Mater. Interfaces* **2015,** *2* (16), 1500360.

20. Smalley, J. F.; Feldberg, S. W.; Chidsey, C. E.; Linford, M. R.; Newton, M. D.; Liu, Y.-P., The kinetics of electron transfer through ferrocene-terminated alkanethiol monolayers on gold. *J. Phys. Chem* **1995,** *99* (35), 13141-13149.

21. Protsailo, L. V.; Fawcett, W. R., Studies of electron transfer through self-assembled monolayers using impedance spectroscopy. *Electrochim. Acta* **2000,** *45* (21), 3497-3505.

22. Franz, M.; Chandola, S.; Koy, M.; Zielinski, R.; Aldahhak, H.; Das, M.; Freitag, M.; Gerstmann, U.; Liebig, D.; Hoffmann, A. K., Controlled growth of ordered monolayers of N-heterocyclic carbenes on silicon. *Nat. Chem.* **2021**, 1-8.

23. Sieval, A. B.; Linke, R.; Heij, G.; Meijer, G.; Zuilhof, H.; Sudhölter, E. J., Amino-terminated organic monolayers on hydrogen-terminated silicon surfaces. *Langmuir* **2001,** *17* (24), 7554-7559.

24. Sun, Q. Y.; de Smet, L. C.; van Lagen, B.; Wright, A.; Zuilhof, H.; Sudhölter, E. J., Covalently Attached Monolayers on Hydrogen-Terminated Si (100): Extremely Mild Attachment by Visible Light. *Angew. Chem.* **2004,** *116* (11), 1376-1379.

25. Buriak, J. M., Organometallic chemistry on silicon surfaces: formation of functional monolayers bound through Si–C bonds. *Chem. Commun.* **1999,** (12), 1051-1060.

26. Hauquier, F.; Ghilane, J.; Fabre, B.; Hapiot, P., Conducting ferrocene monolayers on nonconducting surfaces. *J. Am. Chem. Soc.* **2008,** *130* (9), 2748-2749.

27. Fabre, B., Ferrocene-terminated monolayers covalently bound to hydrogen-terminated silicon surfaces. Toward the development of charge storage and communication devices. *Acc. Chem. Res.* **2010,** *43* (12), 1509-1518.

28. Sieval, A. B.; van den Hout, B.; Zuilhof, H.; Sudhölter, E. J., Molecular modeling of covalently attached alkyl monolayers on the hydrogen-terminated Si (111) surface. *Langmuir* **2001,** *17* (7), 2172-2181.

29. Sieval, A. B.; Opitz, R.; Maas, H. P.; Schoeman, M. G.; Meijer, G.; Vergeldt, F. J.; Zuilhof, H.; Sudhölter, E. J., Monolayers of 1-alkynes on the H-terminated Si (100) surface. *Langmuir* **2000,** *16* (26), 10359-10368.

30. Nguyen, A. T.; Baggerman, J.; Paulusse, J. M.; van Rijn, C. J.; Zuilhof, H., Stable protein-repellent zwitterionic polymer brushes grafted from silicon nitride. *Langmuir* **2011,** *27* (6), 2587-2594.

31. Fabre, B.; Wayner, D. D., Electrochemically directed micropatterning of a conducting polymer covalently bound to silicon. *Langmuir* **2003,** *19* (17), 7145-7146.

32. Schmeltzer, J.; Porter, L. A.; Stewart, M. P.; Buriak, J. M., Hydride abstraction initiated hydrosilylation of terminal alkenes and alkynes on porous silicon. *Langmuir* **2002,** *18* (8), 2971-2974.

33. Wang, D.; Buriak, J. M., Trapping silicon surface-based radicals. *Langmuir* **2006,** *22* (14), 6214-6221.

34. Lin, T.; Wu, Y.; Santos, E.; Chen, X.; Ahn, D.; Mohler, C.; Chen, Z., Molecular Insights into Adhesion at a Buried Silica-Filled Silicone/Polyethylene Terephthalate Interface. *Langmuir* **2020,** *36* (49), 15128-15140.

35. Dief, E. M.; Brun, A. P. L.; Ciampi, S.; Darwish, N., Spontaneous Grafting of OH-Terminated Molecules on Si− H Surfaces via Si–O–C Covalent Bonding. *Surfaces* **2021,** *4* (1), 81-88.

36. Rahpeima, S.; Dief, E. M.; Peiris, C. R.; Ferrie, S.; Duan, A.; Ciampi, S.; Raston, C. L.; Darwish, N., Reduced graphene oxide–silicon interface involving direct Si–O bonding as a conductive and mechanical stable ohmic contact. *Chem. Commun.* **2020,** *56* (46), 6209-6212.

37. Tian, R.; Seitz, O.; Li, M.; Hu, W.; Chabal, Y. J.; Gao, J., Infrared characterization of interfacial Si− O bond formation on silanized flat SiO2/Si surfaces. *Langmuir* **2010,** *26* (7), 4563-4566.

38. Dief, E. M.; Vogel, Y. B.; Peiris, C. R.; Le Brun, A. P.; Gonçales, V. R.; Ciampi, S.; Reimers, J. R.; Darwish, N., Covalent Linkages of Molecules and Proteins to Si–H Surfaces Formed by Disulfide Reduction. *Langmuir* **2020,** *36* (49), 14999-15009.

39. Peiris, C. R.; Ciampi, S.; Dief, E. M.; Zhang, J.; Canfield, P. J.; Le Brun, A. P.; Kosov, D. S.; Reimers, J. R.; Darwish, N., Spontaneous S–Si bonding of alkanethiols to Si (111)–H: towards Si–molecule–Si circuits. *Chem. Sci* **2020,** *11* (20), 5246-5256.

40. Li, Y.-h.; Wang, D.; Buriak, J. M., Molecular layer deposition of thiol− ene multilayers on semiconductor surfaces. *Langmuir* **2010,** *26* (2), 1232-1238.

41. Epping, J. D.; Yao, S.; Karni, M.; Apeloig, Y.; Driess, M., Si□ X Multiple Bonding with Four-Coordinate Silicon? Insights into the Nature of the Si□ O and Si□ S Double Bonds in Stable Silanoic Esters and Related Thioesters: A Combined NMR Spectroscopic and Computational Study. *J. Am. Chem. Soc.* **2010,** *132* (15), 5443-5455.

42. Peiris, C. R.; Vogel, Y. B.; Le Brun, A. P.; Aragonès, A. C.; Coote, M. L.; Díez-Pérez, I.; Ciampi, S.; Darwish, N., Metal–Single-Molecule–Semiconductor Junctions Formed by a Radical Reaction Bridging Gold and Silicon Electrodes. *J. Am. Chem. Soc.* **2019,** *141* (37), 14788-14797.

43. Faber, E. J.; de Smet, L. C.; Olthuis, W.; Zuilhof, H.; Sudhölter, E. J.; Bergveld, P.; van den Berg, A., Si□ C Linked Organic Monolayers on Crystalline Silicon Surfaces as Alternative Gate Insulators. *ChemPhysChem* **2005,** *6* (10), 2153-2166.

44. Rosso, M.; Giesbers, M.; Arafat, A.; Schroën, K.; Zuilhof, H., Covalently Attached Organic Monolayers on SiC and Si x N4 Surfaces: Formation Using UV Light at Room Temperature. *Langmuir* **2009,** *25* (4), 2172-2180.

45. Fabre, B.; Bassani, D. M.; Liang, C.-K.; Ray, D.; Hui, F.; Hapiot, P., Anthracene and anthracene: C60 adduct-terminated monolayers covalently bound to hydrogen-terminated silicon surfaces. *J. Phys. Chem. C* **2011,** *115* (30), 14786-14796.

46. Vogel, Y. B.; Zhang, J.; Darwish, N.; Ciampi, S., Switching of current rectification ratios within a single nanocrystal by facet-resolved electrical wiring. *ACS nano* **2018,** *12* (8), 8071-8080.

47. Dief, E. M.; Darwish, N., Ultrasonic Generation of Thiyl Radicals: A General Method of Rapidly Connecting Molecules to a Range of Electrodes for Electrochemical and Molecular Electronics Applications. *ACS Sens.* **2020,** *6* (2), 573-580.

48. Chai, J.; Wang, D.; Fan, X.; Buriak, J. M., Assembly of aligned linear metallic patterns on silicon. *Nat. Nanotechnol* **2007,** *2* (8), 500-506.

49. Fabre, B.; Hauquier, F.; Herrier, C.; Pastorin, G.; Wu, W.; Bianco, A.; Prato, M.; Hapiot, P.; Zigah, D.; Prasciolu, M., Covalent assembly and micropatterning of functionalized multiwalled carbon nanotubes to monolayer-modified Si (111) surfaces. *Langmuir* **2008,** *24* (13), 6595-6602.

50. Sieval, A. B.; Vleeming, V.; Zuilhof, H.; Sudhölter, E. J., An improved method for the preparation of organic monolayers of 1-alkenes on hydrogen-terminated silicon surfaces. *Langmuir* **1999,** *15* (23), 8288-8291.

51. Rahpeima, S.; Dief, E. M.; Ciampi, S.; Raston, C. L.; Darwish, N., Impermeable Graphene Oxide Protects Silicon from Oxidation. *ACS Appl. Mater. Interfaces* **2021,** *13* (32), 38799-38807.

52. Scheres, L.; Arafat, A.; Zuilhof, H., Self-assembly of high-quality covalently bound organic monolayers onto silicon. *Langmuir* **2007,** *23* (16), 8343-8346.

53. Ciampi, S.; Eggers, P. K.; Le Saux, G.; James, M.; Harper, J. B.; Gooding, J. J., Silicon (100) electrodes resistant to oxidation in aqueous solutions: an unexpected benefit of surface acetylene moieties. *Langmuir* **2009,** *25* (4), 2530-2539.

54. Ciampi, S.; Böcking, T.; Kilian, K. A.; James, M.; Harper, J. B.; Gooding, J. J., Functionalization of acetylene-terminated monolayers on Si (100) surfaces: a click chemistry approach. *Langmuir* **2007,** *23* (18), 9320-9329.

55. Ma, J. W.; Lee, W.-J.; Bae, J. M.; Jeong, K.-S.; Oh, S. H.; Kim, J. H.; Kim, S.-H.; Seo, J.-H.; Ahn, J.-P.; Kim, H., Carrier mobility enhancement of tensile strained Si and SiGe nanowires via surface defect engineering. *Nano Lett.* **2015,** *15* (11), 7204-7210.

56. Darwish, N.; Eggers, P. K.; Ciampi, S.; Tong, Y.; Ye, S.; Paddon-Row, M. N.; Gooding, J. J., Probing the effect of the solution environment around redox-active moieties using rigid anthraquinone terminated molecular rulers. *J. Am. Chem. Soc.* **2012,** *134* (44), 18401-18409.

TOC graphic